Hindawi Publishing Corporation
International Journal of Photoenergy
Volume 2014, Article ID 475713, 8 pages
http://dx.doi.org/10.1155/2014/475713

Research Article

Preparation, Characterization, and Photocatalytic Applications of MWCNTs/TiO_2 Composite

Ahmed M. Kamil,[1] Falah H. Hussein,[1] Ahmed F. Halbus,[1] and Detlef W. Bahnemann[2]

[1] *Chemistry Department, College of Science, University of Babylon, P.O. Box 51002, Hilla, Iraq*
[2] *Institut für Technische Chemie, Leibniz Universität Hannover, Callin Straße 3, 30167 Hannover, Germany*

Correspondence should be addressed to Falah H. Hussein; abohasan_hilla@yahoo.com

Received 8 July 2014; Accepted 1 August 2014; Published 28 August 2014

Academic Editor: Jiaguo Yu

The multiwall carbon nanotubes (MWCNTs)/titanium dioxide (P25) composite in different ratios was prepared using simple evaporation and drying process. The composite was characterized by Raman spectroscopy, X-ray diffraction (XRD), UV-visible diffuse reflectance spectroscopy, and scanning electron microscopy (SEM). The photocatalytic activity of this composite was investigated using degradation of the Bismarck brown R dye (BBR). An optimal MWCNTs/TiO_2 ratio of 0.5% (w/w) was found to achieve the maximum rate of BBR degradation. It was observed that the composite exhibits enhanced photocatalytic activity compared with TiO_2. The enhancement in photocatalytic activity performance of the MWCNTs/P25 composite is explained in terms of recombination of photogenerated electron-hole pairs. In addition, MWCNTs act as a dispersing support to control the morphology of TiO_2 particles in the MWCNTs/TiO_2 composite.

1. Introduction

Titanium dioxide (TiO_2) is photocatalyst material using light to destroy environmental contaminants from wastewater due to its ability to convert them into innocuous end products such as CO_2 and H_2O [1]. TiO_2 is one of the most prominent oxide semiconductor materials due to its high photocatalytic activity, chemical stability, nontoxicity, physical properties, and low cost [2]. However, TiO_2 has some disadvantage such as low surface area and easy recombination of the electron-hole pair [3]. The photocatalytic activity of TiO_2 can be improved by reducing the electron-hole recombination rate, preventing the particles agglomeration, and increasing the adsorption capacity. The photocatalytic efficiency can be enhanced by the modification of TiO_2 surface [4]. Unique properties of carbon nanotubes (CNTs) make them promising material for the fabrication of CNTs/P25 composite for a broad range of applications in photocatalysis [5].

In recent years, titanium dioxide nanoparticles supported on carbon nanotubes have been extensively studied and found to be effective photocatalyst for the removal of hazardous organic chemicals from wastewater. CNTs/TiO_2 nanocomposite can be prepared by different methods which are classified into two basic classes. The first class involves the prior synthesis of TiO_2 nanoparticles thereafter connected to surface functionalized MWCNTs by either covalent or noncovalent interactions [6]. The second class is the one step method which involves direct deposition of TiO_2 nanoparticles onto MWCNTs surface and in situ formation of nanoparticles through redox reactions or electrochemical deposition on CNTs [7, 8]. The important issues that must be considered to obtain composite with enhanced properties are efficient chemical functionalization of CNTs, homogeneous dispersions in solvents, and good interconnectivity with TiO_2. The effective utilization of CNTs in composite applications strongly depends on the ability to disperse them homogeneously. Chemical modifications have become an important issue due to the poor solubility of the CNTs in almost any solvent. Chemical modification of CNTs ensures good dispersion of nanotubes in a medium and enhances interconnectivity with titanium dioxide [9, 10]. After chemical modification or functionalization, the nanotube surface contains polar groups like hydroxyl or carboxyl groups which are able to interact with the oxygen of the titanium dioxide

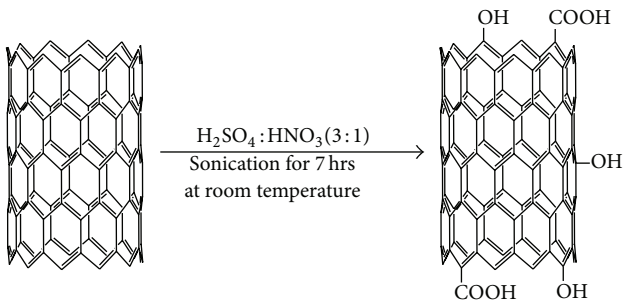

Figure 1: Oxidation of the CNTs by $H_2SO_4 : HNO_3$.

through hydrogen bonding. In CNTs/TiO_2 composite the photocatalytic enhancement is generally attributed to electron capture by the CNTs and in the surface recombination rate [11]. The bond of carbon-oxygen-titanium can extend the light absorption to longer wavelengths and therefore potentially lead to the improvement of the photocatalytic activity [12].

In the present study, MWCNTs/P25 composite was prepared by simple evaporation and drying process. The resultant composite was characterized by Raman spectroscopy, X-ray diffraction (XRD), UV-visible reflectance spectroscopy, and scanning electron microscopy (SEM). The effect of MWCNTs on the optical properties of TiO_2 was observed by measuring the degree of photocatalytic degradation of aqueous Bismarck brown R (BBR) dye solution.

2. Experiment

2.1. Chemicals. Multiwall carbon nanotubes (MWCNTs) and BBR ($C_{21}H_{24}N_8{\cdot}2HCl$) were purchased from Sigma-Aldrich in Germany. For the oxidation of the surfaces of MWCNTs, sulphuric and nitric acid were chosen as the oxidizing agents. These oxidizing agents were purchased from Sigma-Aldrich also. Titanium dioxide was obtained from Degussa AG.

2.2. Functionalization of Multiwall Carbon Nanotubes. 100 mg of MWCNTs was suspended in 50 mL of a 3 : 1 mixture of concentrated H_2SO_4/HNO_3. The MWCNTs suspension was sonicated in a water bath for 7 hrs at room temperature to open the agglomeration of the nanotubes and to anchor the acid solution uniformly on the carbon's surface. Figure 1 shows the oxidation of the CNTs. The resultant suspension was then diluted with 1000 mL of distilled water. The oxidized MWCNTs were filtered and washed several times with distilled water by centrifuge. A dialysis process was used to obtain a neutral pH, and then the oxidized MWCNTs were dried at 100°C for 10 hrs.

2.3. Synthesis of the Composite. Different ratios from the MWCNTs/P25 composite were prepared using a simple evaporation and drying process. That is, commercial titanium dioxide (P25) and O-MWCNTs were dispersed into 100 and 20 mL of distilled water and sonicated for 30 and 15 min, respectively. The O-MWCNTs solution was added to the TiO_2 suspension along with stirring. The suspension containing MWCNTs and TiO_2 particles was heated to 80°C to evaporate the water. After the water had evaporated, the composite was dried overnight in an oven at 100°C. Figure 2 shows the experimental procedure for preparation of the MWCNTs/P25 composite by using simple evaporation and drying process.

2.4. Characterization Methods. X-ray diffraction (XRD) spectra were collected on a STADI P diffractometer (STOE, Germany) with a positional sensitive detector using monochromatic Cu Kα radiation.

XRD data were employed to calculate the mean crystallite sizes (D) by Scherrer's formula in the following equation [13]:

$$D = \frac{k\lambda}{\beta \cos\theta} \tag{1}$$

where D is the average crystal size, $k = 0.94$ is the constant crystal lattice, $\lambda = 0.154$ nm is the X-ray wavelength of Cu Kα, β is the full width of the peak measured at half maximum intensity, and θ is Bragg's angle of the peak.

Band gap energies of P25 and MWCNTs/P25 composites were determined via the measurement of reflectance data R using a Cary 100 Scan UV-visible spectrophotometer system. This is equipped with a Labsphere integrating sphere diffusing reflectance accessory for diffuse reflectance spectra by employing $BaSO_4$ as a reference material. The measured reflectance data (R) were transformed to the Kubelka-Munk function $F(R)$ by the following equations [14]:

$$F(R) = \frac{(1-R)^2}{2R}$$
$$[F(R) \cdot E]^{1/2} = \left[\frac{(1-R)^2}{2R} \cdot E\right]^{1/2}. \tag{2}$$

The band gap energy for all the samples was measured from the plot of $(F(R) \cdot E)^{1/2}$ versus (E) energy of light ($h\nu$) in eV. This depended on the intersection of the tangent via the point of inflection in the absorption band and the photon energy axis.

Scanning electron microscopy (SEM) measurements were carried out on a JEOL JSM-6700F instrument, using a secondary electron detector (SE) at an accelerating voltage of 2.0 kV.

2.5. Photocatalytic Activity. The photocatalytic activity of MWCNTs/P25 composite was determined using BBR decomposition in aqueous solution under an UV lamp (0.7 mW/cm^2). The suspensions solutions were prepared by adding 50 mg of nanocomposite catalysts to 100 mL of 5×10^{-5} M BBR aqueous solution. Prior to irradiation, the suspensions were stirred in darkness for 30 min using a magnetic stirrer to ensure adsorption equilibrium. During adsorption and irradiation, the suspensions were sampled at regular intervals. 3 mL of the reaction mixture was collected and centrifuged for 15 min. The clear solution was carefully removed using a syringe and centrifuged again at the same speed and the same period time. The second centrifuge was

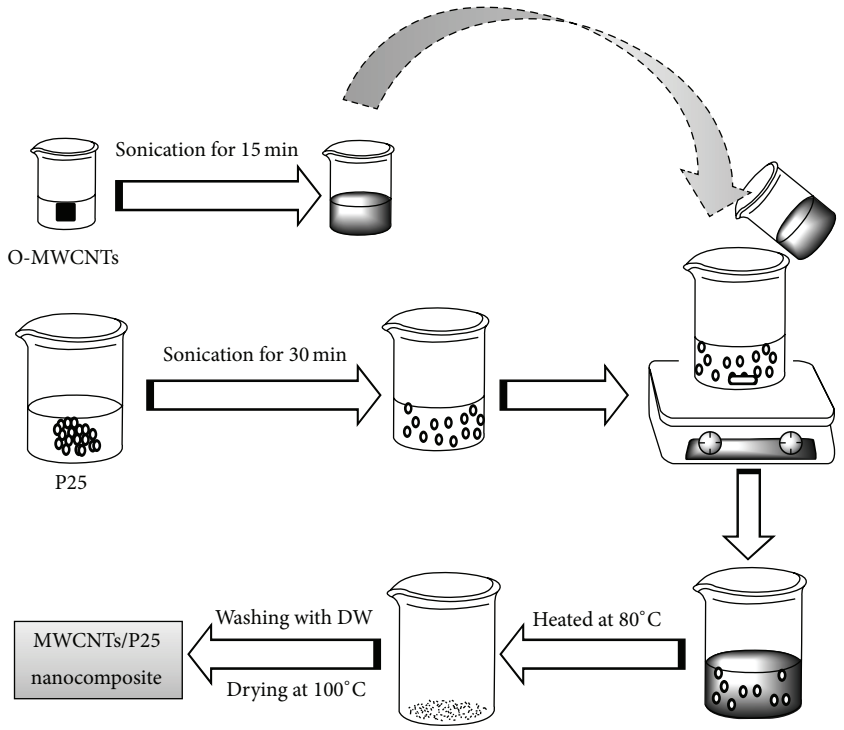

Figure 2: Schematic diagram of the experimental procedure for the preparation of the MWCNTs/P25 composite by using simple evaporation and drying process.

found necessary to remove fine particles of the catalyst. After the second centrifuge, the absorbance at the maximum wavelength of 459 nm of the BBR was measured with a UV-visible spectrophotometer.

The photocatalytic reactions on the surfaces of MWCNTs/P25 composites can be expressed by the Langmuir-Hinshelwood model. The rate of the photocatalytic reaction can be expressed as

$$\ln\left(\frac{C_0}{C_t}\right) = kt, \tag{3}$$

where C_t and C_0 are the reactant concentration at time $t = t$ and $t = 0$, respectively, and k and t are the apparent reaction rate constant and time, respectively. A plot of $\ln(C_0/C_t)$ versus t will yield a slope of k.

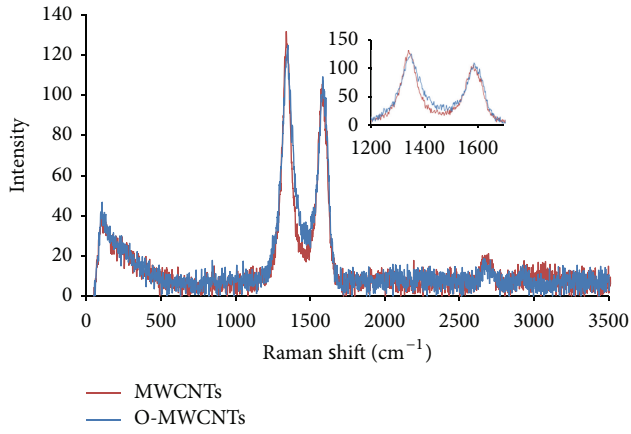

Figure 3: Raman spectra for MWCNTs and O-MWCNTs.

3. Results and Discussion

3.1. Characterization of the MWCNTs/P25 Composite. Raman spectra for MWCNTs and O-MWCNTs are shown in Figure 3. Three distinct bands found in the MWCNTs Raman spectrum, which originate from different aspects of the nanotube, are the radial breathing mode (RBM), the disordered mode (D mode), and the tangential mode (G band) [15]. For MWCNTs, the radial breathing mode at 105 cm^{-1} depends on the tube's diameter. The shape and intensity of the D mode at 1340 cm^{-1} correspond to the sp^3 hybridized carbon atoms [16], which is correlated with the extent of the nanotubes sidewall defects and the chemical sidewall functionalization. The higher frequency tangential G mode at 1574 cm^{-1} and the first overtone of the D band, which is called the G' band at 2694 cm^{-1}, are sensitive to the charge exchanged between the nanotubes and the guest moiety. The G band is thus an intrinsic feature of carbon nanotubes, which is closely related to vibrations in all sp^2 carbon materials. The second order G' band does not require an elastic defect-related scattering process and is observable for defect-free sp^2 carbons. Chemical oxidation produces defects on the sidewalls of the nanotubes and attaches some functional groups onto the defective areas of the nanotubes. In the Raman spectrum of the O-MWCNTs, these bands were shifted to 106.5, 1350.5, 1584, and

Table 1: A comparison of the Raman spectra features of the pristine and functionalized MWCNTs samples.

Sample	I_D/I_G	FWHM (cm^{-1})	
		G band ($\Delta\omega_G$)	D band ($\Delta\omega_D$)
MWCNTs	1.2748	77.1494	70.0351
O-MWCNTs	1.1437	42.8988	91.8137

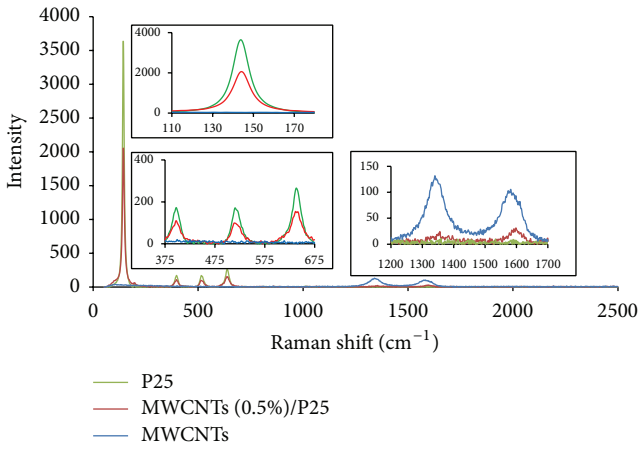

Figure 4: Raman spectra for P25, MWCNTs (0.5%)/P25, and MWCNTs.

$2662.5\,cm^{-1}$ for the RBM, D, G, and for the first overtone of the D bands, respectively. Also, the results indicate that the intensity of the G mode slightly increased, while the D mode intensity decreased after oxidative treatment. The ratio of the D to the G band intensity (I_D/I_G) is usually used for a measurement of the disordered sites on carbon nanotubes walls and it is the indicator of the level of the covalent functionalization of the MWCNTs [17]. On comparing the modified and nonmodified tubes a decrease in the ratio of intensities I_D/I_G from 1.2748 to 1.1437 was observed because of the elimination of amorphous carbon during the acid treatment on the modified tubes as is shown in Table 1. The full width at half the maximum (FWHM) of the D and G bands was analyzed for pristine and functionalized samples of MWCNTs (Table 1). For the D peak, the FWHM of the functionalized MWCNTs ($\Delta\omega_D = 91.8137\,cm^{-1}$) was much larger than that of the untreated MWCNTs ($\Delta\omega_D = 70.0351\,cm^{-1}$), and for G peak, the FWHM of the functionalized MWCNTs ($\Delta\omega_G = 42.8988\,cm^{-1}$) was smaller than that of the untreated MWCNTs ($\Delta\omega_G = 77.1494\,cm^{-1}$). The results are in good agreement with [18]. Table 1 shows a comparison of the Raman spectra features of the pristine and functionalized MWCNTs samples.

Raman spectroscopy was used to investigate the interaction of titanium dioxide P25 with the MWCNTs. The spectra of the P25, MWCNTs, and MWCNTs (0.5%)/P25 composite are illustrated in Figure 4. The characteristic bands at 144, 197, 397.5, 515.5, and $638.5\,cm^{-1}$ correspond to the anatase phase of the P25 [19]. The main four bands (197, 397.5, 515.5, and $638.5\,cm^{-1}$) in the Raman spectrum are representative of the anatase P25 being broadened and shifted to 195.5, 397,

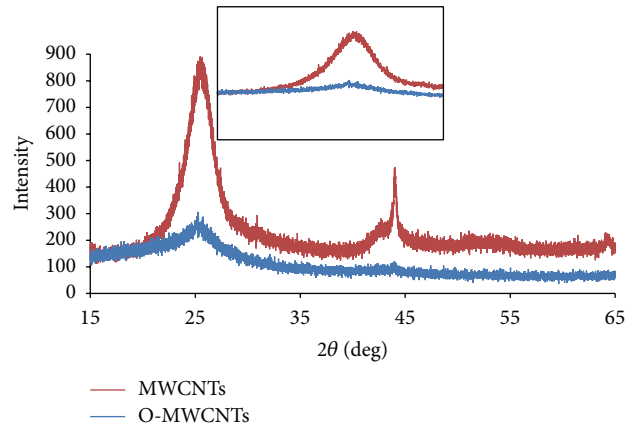

Figure 5: XRD for MWCNTs and O-MWCNTs.

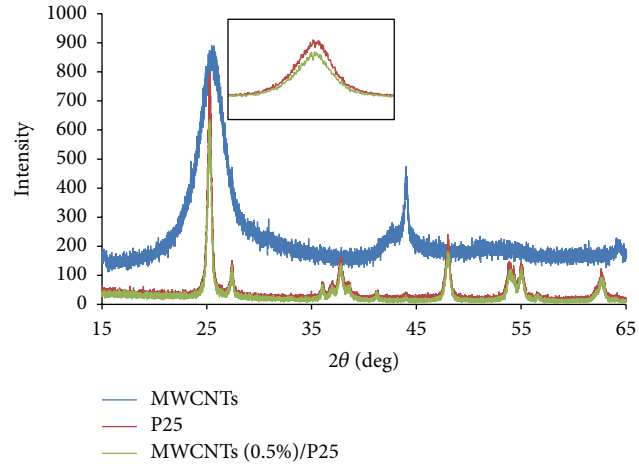

Figure 6: XRD for the MWCNTs, P25, and MWCNTs (0.5%)/P25 composites.

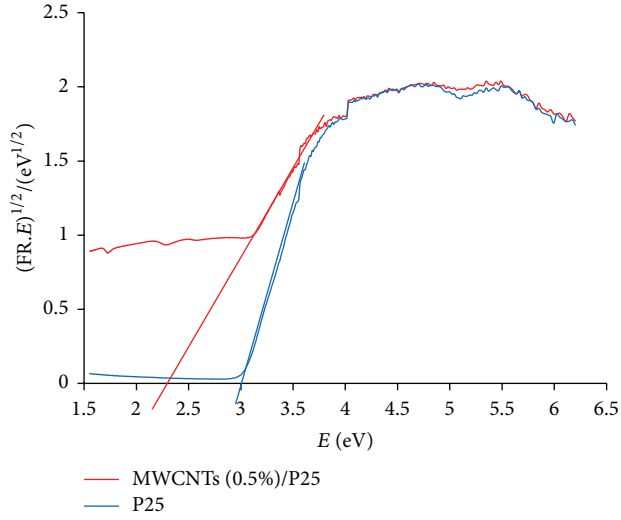

Figure 7: UV-visible Kubelka-Munk transformed diffuse reflectance spectra of P25 and MWCNTs/P25 composites.

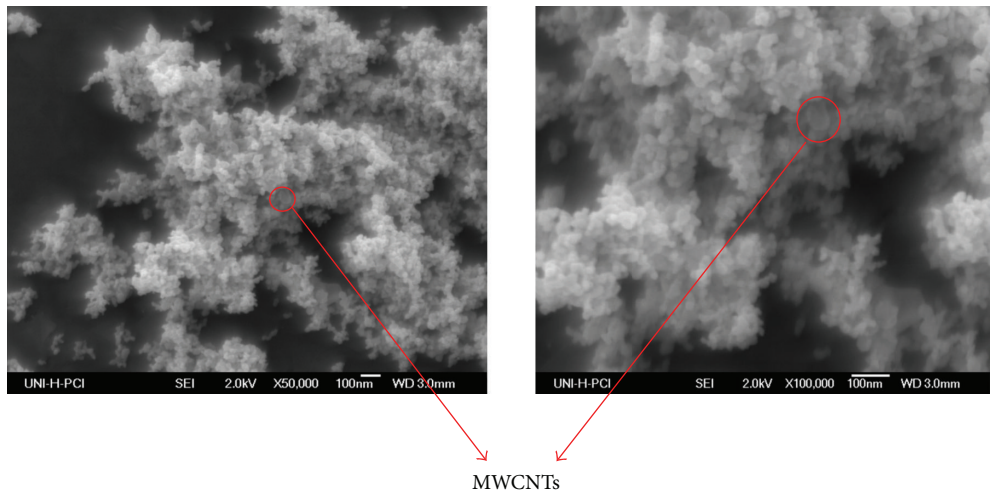

Figure 8: SEM images of the MWCNTs (0.5%)/P25 composite.

514, and 637 cm^{-1} in MWCNTs/P25 composite, as compared to the pure P25. The band broadening and decreasing in intensity can be attributed to the effects of smaller particle sizes [20, 21]. The composite sample shows the D and G bands of MWCNTs. These bands shift to 1356 and 1598.5 cm^{-1} in the MWCNTs/P25 composite, clearly indicating that the strong interaction between the P25 and the MWCNTs may enhance a charge transfer from the P25 to the MWCNTs in order to separate and stabilize the charge and thereby hinder charge recombination [22–24].

XRD characterization method is used to measure the extent of graphitization, as well as providing information about the degree of nanotube alignment. Figure 5 shows comparison between the X-ray diffraction of the MWCNTs and the O-MWCNTs. The pattern of the O-MWCNTs shows a high intense peak at $2\theta = 24.6^{\circ}$ and a low intense peak at $2\theta = 43.9^{\circ}$, corresponding to the (002) and (100) reflections, respectively. Compared to the MWCNTs, $2\theta = 25.2^{\circ}$ and $2\theta = 44.0^{\circ}$, these peaks show a downward shift, which is attributed to an increase in the sp^2 C=C layers spacing [25] and suggests that crystallinity is not lost due to oxidative acid treatment. Furthermore, the XRD patterns were used to characterize the crystalline structure of the MWCNT/P25 composites. Figure 6 shows the XRD patterns of the P25 compared with the MWCNT/P25 composite. The patterns demonstrate the highly crystalline nature of the composite. The same peaks in P25 and composite at 25.3°, 37.8°, 48.0°, 54.9°, and 62.5° were the diffractions of (101), (004), (200), (211), and (204) planes off anatase, respectively, and peaks at 27.4°, 36.1°, 41.2°, and 54.3° belonging to the diffraction peaks of (110), (101), (111), and (211) planes of rutile, thus indicating that the P25 and the composite contain a mixed structure of anatase and rutile. It was also observed that the MWCNTs/P25 composite had a weaker intensity compared with the P25. When comparing the XRD patterns of the MWCNTs and the MWCNTs/P25 composites, the characteristic peaks for the MWCNTs at the positions of 25.2° and 44.0° might disappear or become thinner in the XRD pattern of the composites. The reason for this is that these peaks in the composites overlapped with the main peak of the anatase phase of the P25 at 25.3°.

The crystalline extent of the MWCNTs is lower than the crystalline extent of the P25, leading to the shielding of the peaks of the MWCNTs by those of TiO_2. Also, the small C content in the composite, as well as the absence of MWCNTs aggregated in the pores, was supported by the disappearance of the characteristic peaks from the MWCNTs in the XRD patterns [26]. The average crystallite sizes of the P25 and MWCNTs/P25 composite were calculated by Debye-Scherer formula. According to the calculation, the average crystallite sizes of the P25 and composite were 22.7 and 21.4 nm, respectively [27].

The results of the UV-visible diffuse reflectance spectra of the P25 and the composite, as well as UV-visible Kubelka-Munk transformed diffuse reflectance spectra, indicate that the band gap of the P25 is wider than that of the MWCNTs/P25 composite. Figure 7 shows the optical absorption spectra of the P25 and the MWCNTs (0.5%)/P25 composite. The MWCNTs/P25 composite can exhibit better absorbency than the P25 within a wavelength region of 200–800 nm. Compared with the P25, the MWCNTs/P25 composite particles can cause an obvious red shift of the UV-visible spectra. The P25 particles are clearly absorbed at wavelengths above 380 nm by adding MWCNTs to obtain MWCNTs/P25 composites. The effective band gap of the P25 3.0 eV is reduced to 2.3 eV for MWCNTs (0.5%)/P25. Therefore the MWCNTs/P25 composite can be excited to produce more electron-hole pairs under solar irradiation, which may result in higher photocatalytic activity. For all the composites, their enhanced absorbance extends broadly over wavelengths of >400 nm, which is in agreement with the black color of the sample [28–30].

The morphology of the MWCNTs/P25 composite was studied using an SEM, as shown in Figure 8. The SEM images indicate that the MWCNTs are homogenously distributed throughout the P25 matrix with an apparent agglomeration of the P25 particles. An explanation was provided that the thorough dispersion of the small MWCNTs particles into the P25 aggregates could provide the information on the presence of more reactive sites, due to a considerable portion of the P25 being enclosed in the three-dimensional matrix. So it was

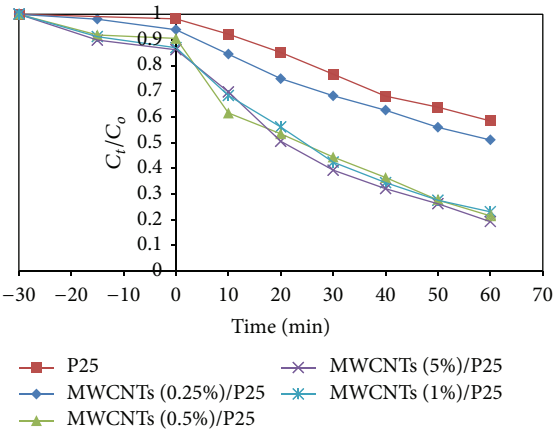

Figure 9: Adsorption and irradiation at different ratios of the MWCNTs/P25 composite.

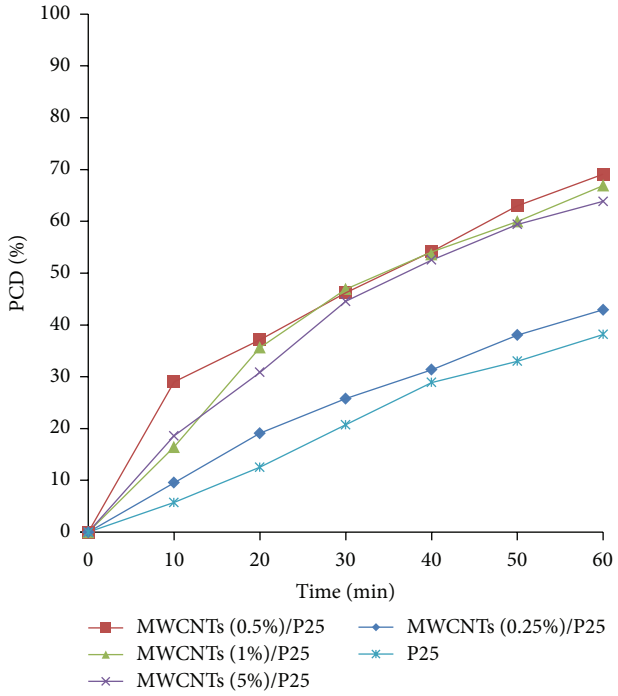

Figure 10: The photocatalytic decolorization percentage of the BBR dye at different ratios of the prepared MWCNTs/P25 composite.

considered that the MWCNTs/P25 composite could show much more activity, including an excellent photocatalytic activity. The average sizes of the catalyst particles were 25.1 nm, which agrees with the XRD measurements [31–33].

3.2. Photocatalytic Activity of the MWCNTs/P25 Composite. The photocatalytic removal of the BBR aqueous solution was investigated using a source of UV light irradiation. Figure 9 shows the changes in relative concentration of the BBR in aqueous solution on UV irradiation times for the MWCNTs/P25 composite in different ratios. The results indicate that the MWCNTs enhanced the adsorption properties of TiO_2 (P25) due to enhancement in surface area [34, 35]. After 60 min of UV irradiation, the MWCNTs (0.5%)/P25 in

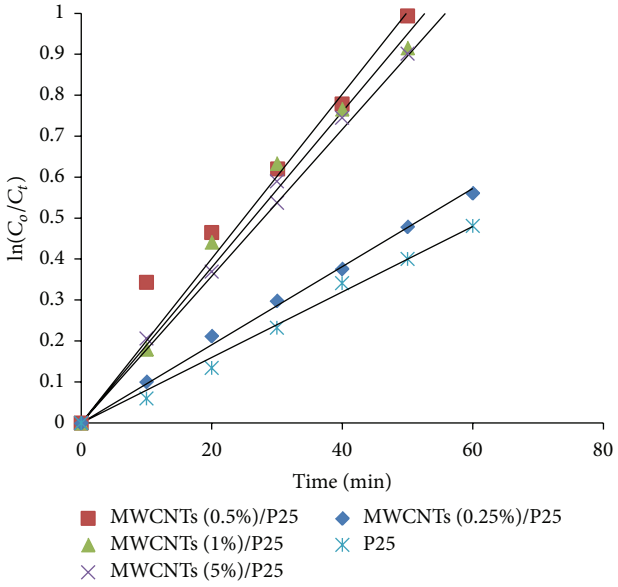

Figure 11: The changes of $\ln C_o/C_t$ according to irradiation times at different ratios of the prepared MWCNTs/P25 composite.

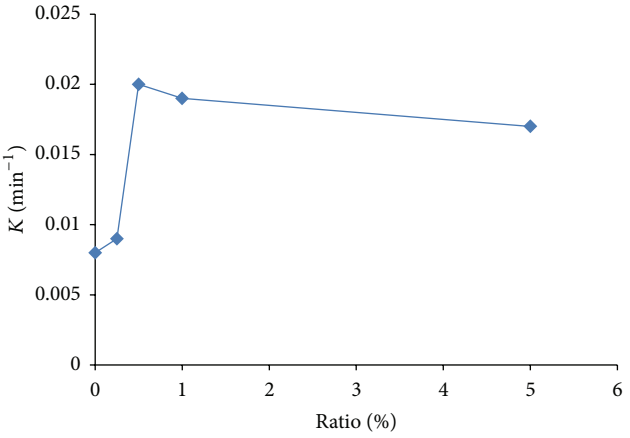

Figure 12: The enhancement of the rate constant of the P25 by MWCNTs with different ratios.

Figure 10 had the highest degradation of the BBR solution, from which 69% was almost removed. The BBR degradation of the P25, MWCNTs (0.25%)/P25, MWCNTs (1%)/P25, and MWCNTs (5%)/P25 also achieved 38, 42, 66, and 63%, respectively. It clearly indicates that all ratios of MWCNTs favor the separation of photogenerated electron-hole pairs and decrease of their recombination rate and thus display significantly enhanced photocatalytic activity for degrading BBR dye in aqueous solution under UV irradiation due to the chemically bonded between P25 and MWCNTs, as compared with commercial P25 photocatalyst [36].

The photocatalytic degradation of the BBR in aqueous suspension of the composite catalysts containing MWCNTs and P25 follows apparent first order kinetics. The kinetic plots are shown in Figures 11 and 12.

4. Conclusions

The MWCNTs/P25 composite photocatalysts with different ratios were prepared using simple evaporation and drying process. Composite characterization indicates a relatively homogeneous MWCNTs dispersion in the P25 matrix with modified UV-visible absorption properties, suggesting a strong interphase structure effect between the MWCNTs and the P25 in the composite. According to the results it could be suggested that all of the samples had a good photocatalytic activity for the BBR degradation. The rate constant for the photodegradation of BBR dye by the P25 increased by 2.5 times in the presence of the 0.5% MWCNTs. The MWCNTs (0.5%)/P25 composite had higher activity of about 2 times than that of the P25 alone. The enhanced photocatalytic efficiency of composite suggests that the MWCNTs act as an adsorbent, dispersing agent and electron reservoir to trap electrons from the P25 particles due to UV irradiation and hence hindering the electron-hole pair recombination.

Conflict of Interests

The authors declare that there is no conflict of interests regarding the publication of this paper.

Acknowledgment

The authors wish to thank Professor Dr. Detlef W. Bahnemann group in the Institute of Technical Chemistry, Leibniz Universität Hannover, Germany, for their assistance.

References

[1] F. H. Hussein and A. F. Halbus, "Rapid decolorization of cobalamin," *International Journal of Photoenergy*, vol. 2012, Article ID 495435, 9 pages, 2012.

[2] F. F. Karam, F. H. Hussein, S. J. Baqir, A. F. Halbus, R. Dillert, and D. Bahnemann, "Photocatalytic degradation of anthracene in closed system reactor," *International Journal of Photoenergy*, vol. 2014, Article ID 503825, 6 pages, 2014.

[3] L. M. Ahmed, I. Ivanova, F. H. Hussein, and D. W. Bahnemann, "Role of platinum deposited on TiO_2 in photocatalytic methanol oxidation and dehydrogenation reactions," *International Journal of Photoenergy*, vol. 2014, Article ID 503516, 9 pages, 2014.

[4] M. Qamar, B. Merzougui, D. Anjum, A. S. Hakeem, Z. H. Yamani, and D. Bahnemann, "Synthesis and photocatalytic activity of mesoporous nanocrystalline Fe-doped titanium dioxide," *Catalysis Today*, vol. 230, pp. 158–165, 2014.

[5] X. Peng, M. Y. Sfeir, F. Zhang, J. A. Misewich, and S. S. Wong, "Covalent synthesis and optical characterization of double-walled carbon nanotube-nanocrystal heterostructures," *Journal of Physical Chemistry C*, vol. 114, no. 19, pp. 8766–8773, 2010.

[6] H. Wu, C. M. Ma, Y. Yang, H. Kuan, C. Yang, and C. Chiang, "Morphology, electrical resistance, electromagnetic interference shielding and mechanical properties of functionalized MWNT and poly(urea urethane) nanocomposites," *Journal of Polymer Science B: Polymer Physics*, vol. 44, no. 7, pp. 1096–1105, 2006.

[7] M. L. Shofner, V. N. Khabashesku, and E. V. Barrera, "Processing and mechanical properties of fluorinated single-wall carbon nanotube-polyethylene composites," *Chemistry of Materials*, vol. 18, no. 4, pp. 906–913, 2006.

[8] P. Poncharal, C. Berger, Y. Yi, Z. L. Wang, and W. A. De Heer, "Room temperature ballistic conduction in carbon nanotubes," *Journal of Physical Chemistry B*, vol. 106, no. 47, pp. 12104–12118, 2002.

[9] W. Tang, M. H. Santare, and S. G. Advani, "Melt processing and mechanical property characterization of multi-walled carbon nanotube/high density polyethylene (MWNT/HDPE) composite films," *Carbon*, vol. 41, no. 14, pp. 2779–2785, 2003.

[10] D. Baskaran, J. W. Mays, and M. S. Bratcher, "Noncovalent and nonspecific molecular interactions of polymers with multiwalled carbon nanotubes," *Chemistry of Materials*, vol. 17, no. 13, pp. 3389–3397, 2005.

[11] K. Woan, G. Pyrgiotakis, and W. Sigmund, "Photocatalytic carbon-nanotube-TiO_2 composites," *Advanced Materials*, vol. 21, no. 21, pp. 2233–2239, 2009.

[12] C. H. Wu, C. Y. Kuo, and S. T. Chen, "Synergistic effects between TiO_2 and carbon nanotubes (CNTs) in a TiO_2/CNTs system under visible light irradiation," *Environmental Technology*, vol. 34, pp. 2513–2519, 2013.

[13] P. Scherrer, "Bestimmung der Grösse und der Inneren Struktur von Kolloidteilchen Mittels Röntgenstrahlen, Nachrichten von der Gesellschaft der Wissenschaften, Göttingen," *Mathematisch-Physikalische Klasse*, vol. 2, pp. 98–100, 1918.

[14] P. Kubelka and F. Munk, "Ein Beitrag zur Optik der Farbanstriche," *Zeitschrift für Technische Physik*, vol. 12, pp. 593–601, 1931.

[15] R. Graupner, "Raman spectroscopy of covalently functionalized single-wall carbon nanotubes," *Journal of Raman Spectroscopy*, vol. 38, no. 6, pp. 673–683, 2007.

[16] D. J. Nelson, H. Rhoads, and C. Brammer, "Characterizing covalently sidewall-functionalized SWNTs," *Journal of Physical Chemistry C*, vol. 111, no. 48, pp. 17872–17878, 2007.

[17] S. Mirershadi, S. Z. Mortazavi, A. Reyhani, N. Moniri, and A. J. Novinrooz, "Effective condition for purification of multi-walled carbon nanotubes by nitric acid," *Synthesis and Reactivity in Inorganic, Metal-Organic and Nano-Metal Chemistry*, vol. 39, no. 4, pp. 204–208, 2009.

[18] M. S. Tehrani, P. A. Azar, P. E. Namin, and S. M. Dehaghi, "Removal of lead ions from aqueous solution using multi-walled carbon nanotubes: the effect of functionalization," *Journal of Applied Environmental and Biological Sciences*, vol. 4, no. 2, pp. 316–326, 2014.

[19] L. N. Dlamini, R. W. Krause, G. U. Kulkani, and S. H. Durbach, "Photodegradation of bromophenol blue with fluorinated TiO_2 composite," *Applied Water Science*, vol. 1, pp. 19–24, 2011.

[20] H. C. Choi, Y. M. Jung, and S. B. Kim, "Characterization of raman spectra of size-selected TiO_2 nanoparticles by two-dimensional correlation spectroscopy," *Bulletin of the Korean Chemical Society*, vol. 25, no. 3, pp. 426–428, 2004.

[21] Y. Xie, S. H. Heo, S. H. Yoo, G. Ali, and S. O. Cho, "Synthesis and photocatalytic activity of anatase TiO_2 nanoparticles-coated carbon nanotubes," *Nanoscale Research Letters*, vol. 5, no. 3, pp. 603–607, 2010.

[22] C. Dechakiatkrai, J. Chen, C. Lynam, S. Phanichphant, and G. G. Wallace, "Photocatalytic oxidation of methanol using titanium dioxide/single-walled carbon nanotube composite," *Journal of the Electrochemical Society*, vol. 154, no. 5, pp. A407–A411, 2007.

[23] B. Réti, K. Mogyorósi, A. Dombi, and K. Hernádi, "Substrate dependent photocatalytic performance of TiO_2/MWCNT photocatalysts," *Applied Catalysis A: General*, vol. 469, pp. 153–158, 2014.

[24] T. Jia, F. Fu, J. Zhao et al., "Sonochemical synthesis, characterization, and photocatalytic activity of N-Doped TiO_2 nanocrystals with mesoporous structure," *International Journal of Photoenergy*, vol. 2014, Article ID 516806, 7 pages, 2014.

[25] H. Zhang, G. Lin, Z. Zhou, X. Dong, and T. Chen, "Raman spectra of MWCNTs and MWCNT-based H_2 adsorbing system," *Carbon*, vol. 40, no. 13, pp. 2429–2436, 2002.

[26] Y. Yu, J. C. Yu, Y. Kwok et al., "Enhancement of photocatalytic activity of mesoporous TiO_2 by using carbon nanotubes," *Applied Catalysis A: General*, vol. 289, no. 2, pp. 186–196, 2005.

[27] F. K. M. Alosfur, M. H. H. Jumali, S. Radiman, N. J. Ridha, and A. A. Umar, " In-situ dressing of MWCNTs with TiO_2 nanoparticles: microwave-assisted synthesis towards water treatment," *Procedia Technology*, vol. 12, pp. 264–270, 2014.

[28] Z. R. Tang, F. Li, Y. Zhang, X. Fu, and Y. J. Xu, "Composites of titanate nanotube and carbon nanotube as photocatalyst with high mineralization ratio for gas-phase degradation of volatile aromatic pollutant," *Journal of Physical Chemistry C*, vol. 115, no. 16, pp. 7880–7886, 2011.

[29] C. Wu, C. Kuo, and S. Chen, "Synergistic effects between TiO_2 and carbon nanotubes (CNTs) in a TiO_2/CNTs system under visible light irradiation," *Environmental Technology*, vol. 34, pp. 2513–2519, 2013.

[30] H. Liu, H. Zhang, and H. Yang, "Photocatalytic removal of nitric oxide by multi-walled carbon nanotubes-supported TiO_2," *Chinese Journal of Catalysis*, vol. 35, pp. 66–77, 2014.

[31] S. J. Kim, J. S. Im, P. H. Kang, T. Kim, and Y. S. Lee, "Photo catalytic activity of CNT-TiO_2 nanocomposite in degrading anionic and cationic dyes," *Carbon Letters*, vol. 9, no. 4, pp. 294–297, 2008.

[32] B. K. Vijayan, N. M. Dimitrijevic, D. Finkelstein-Shapiro, J. Wu, and K. A. Gray, "Coupling titania nanotubes and carbon nanotubes to create photocatalytic nanocomposites," *ACS Catalysis*, vol. 2, no. 2, pp. 223–229, 2012.

[33] X. Huang, M. Feng, and X. Liu, "Design of bristle-like TiO_2-MWCNT nanotubes to improve the dielectric and interfacial properties of polymer-based composite films," *RSC Advances*, vol. 4, pp. 4985–4992, 2014.

[34] F. Alosfur, M. H. H. Jumali, S. Radiman, N. J. Ridha, M. A. Yarmo, and A. A. Umar, "Visible light-responsive TiO_2 coated MWCNTs as a hybrid nanocatalysts," *International Journal of Electrochemical Science*, vol. 8, pp. 2977–2982, 2013.

[35] C. Li and W. Wang, "Photocatalytic degradation of phenol over MWCNTs-TiO_2 composite catalysts with different diameters," *Chinese Journal of Chemical Physics*, vol. 22, no. 4, pp. 423–428, 2009.

[36] J. Yu, T. Ma, and S. Liu, "Enhanced photocatalytic activity of mesoporous TiO_2 aggregates by embedding carbon nanotubes as electron-transfer channel," *Physical Chemistry Chemical Physics*, vol. 13, no. 8, pp. 3491–3501, 2011.